• Basic Research •

Yes-associated protein promotes endothelial-to-mesenchymal transition of endothelial cells in choroidal neovascularization fibrosis

Rong Zou[1], Yi-Fan Feng[1], Ya-Hui Xu[1], Min-Qian Shen[1], Xi Zhang[1], Yuan-Zhi Yuan[1,2]

[1]Department of Ophthalmology, Zhongshan Hospital, Fudan University, Shanghai 200032, China
[2]Department of Ophthalmology, Xiamen Branch, Zhongshan Hospital, Fudan University, Xiamen 361015, Fujian Province, China
Co-first authors: Rong Zou and Yi-Fan Feng
Correspondence to: Yuan-Zhi Yuan. Department of Ophthalmology, Zhongshan Hospital, Fudan University, Shanghai 200032, China. yktgyx2019@163.com
Received: 2021-10-25 Accepted: 2021-12-17

Abstract

● **AIM:** To reveal whether and how Yes-associated protein (YAP) promotes the occurrence of subretinal fibrosis in age-related macular degeneration (AMD).

● **METHODS:** Cobalt chloride ($CoCl_2$) was used in primary human umbilical vein endothelial cells (HUVECs) to induce hypoxia *in vitro*. Eight-week-old male C57BL/6J mice weighing 19-25 g were used for a choroidal neovascularization (CNV) model induced by laser photocoagulation *in vivo*. Expression levels of YAP, phosphorylated YAP, mesenchymal markers [α smooth muscle actin (α-SMA), vimentin, and Snail], and endothelial cell markers (CD31 and zonula occludens 1) were measured by Western blotting, quantitative real-time PCR, and immunofluorescence microscopy. Small molecules YC-1 (Lificiguat, a specific inhibitor of hypoxia-inducible factor 1α), CA3 (CIL56, an inhibitor of YAP), and XMU-MP-1 (an inhibitor of Hippo kinase MST1/2, which activates YAP) were used to explore the underlying mechanism.

● **RESULTS:** $CoCl_2$ increased expression of mesenchymal markers, decreased expression of endothelial cell markers, and enhanced the ability of primary HUVECs to proliferate and migrate. YC-1 suppressed hypoxia-induced endothelial-to-mesenchymal transition (EndMT). Moreover, hypoxia promoted total expression, inhibited phosphorylation, and enhanced the transcriptional activity of YAP. XMU-MP-1 enhanced hypoxia-induced EndMT, whereas CA3 elicited the opposite effect. Expression of YAP, α-SMA, and vimentin were upregulated in the laser-induced CNV model. However, silencing of YAP by vitreous injection of small interfering RNA targeting YAP could reverse these changes.

● **CONCLUSION:** The findings reveal a critical role of the hypoxia-inducible factor-1α (HIF-1α)/YAP signaling axis in EndMT and provide a new therapeutic target for treatment of subretinal fibrosis in AMD.

● **KEYWORDS:** endothelial-to-mesenchymal transition; Yes-associated protein; hypoxia-inducible factor-1α; choroidal neovascularization; age-related macular degeneration

DOI:10.18240/ijo.2022.05.03

Citation: Zou R, Feng YF, Xu YH, Shen MQ, Zhang X, Yuan YZ. Yes-associated protein promotes endothelial-to-mesenchymal transition of endothelial cells in choroidal neovascularization fibrosis. *Int J Ophthalmol* 2022;15(5):701-710

INTRODUCTION

Age-related macular degeneration (AMD), the main cause of permanent blindness in people aged over 60y worldwide, is expected to impart a heavy burden on public health in the next few decades. Exudative (wet) AMD involves fibrovascular proliferation under the central retina (macula), which occurs with characteristic choroidal neovascularization (CNV)[1]. Clinically, anti-vascular endothelial growth factor (VEGF) agents such as bevacizumab, ranibizumab, and aflibercept, have been used to suppress neovascularization in wet AMD. However, a lack of long-term improvements in vision, secondary inflammation, or other side effects considerably limits the usefulness of these treatments[2]. Advanced subretinal fibrosis is considered an important reason for the resistance of wet AMD to anti-VEGF drugs[3].

Endothelial-to-mesenchymal transition (EndMT) has been established in the pathogenesis and progression of many human conditions, including fibrosis of the heart[4], lung[5], liver[6], and kidney[7]. Considered one of the important factors for inducing EndMT, hypoxia can lead to increased expression of mesenchymal marker proteins α smooth muscle actin (α-SMA) and fibroblast-specific protein 1 in rat microvascular endothelial cells[4]. Hypoxia can also lead to

significantly decreased expression of the endothelial marker CD31 and significantly increased expression of mesenchymal markers α-SMA, collagen 1A1 (COL1A1), and COL3A1 in the pulmonary microvascular endothelium[8]. Hypoxia-inducible factor-1α (HIF-1α), a regulator of hypoxia-induced transcription, has been identified as a key molecule that promotes EndMT by regulating transforming growth factor β (TGF-β)/SMAD[8], c-Met/ETS-1[9], and/or nuclear factor κB[10] signaling pathways.

The Hippo pathway is an evolutionarily conserved kinase cascade[11]. Yes-associated protein (YAP) can be phosphorylated by mammalian Ste20-like kinases 1/2 (Mst1/2) and large tumor suppressor 1/2, which prevent its entry into the nucleus to promote transcription of target proteins[12]. Many previous studies demonstrated crucial effects of YAP on epithelial-to-mesenchymal transition (EMT) and tumor cell metastasis. In colorectal cancer cells, YAP was associated with expression of EMT markers and influenced tumor cell migration and invasion[13]. In lung cancer, WW and C2 domain-containing protein 3 inhibited EMT by activating Hippo-YAP signaling[14], and YAP enhanced EMT through feedback regulation of WT1 and Rho family GTPases[15]. These YAP-dependent feedback loops result in switch-like changes in expression of signaling and EMT-related markers[15]. More recently, several studies reported that YAP overexpression in endothelial cells is responsible for EndMT and organ fibrosis, although the exact molecular mechanism still needs to be elucidated[16-18].

Endothelial cells become dysfunctional under hypoxic conditions[19], but whether YAP takes part in hypoxia-induced EndMT and subretinal fibrosis associated with wet AMD is unclear. To clarify the role of YAP in HIF-1α-induced EndMT, the present study employed an *in vitro* hypoxia model involving exposure of human umbilical vein endothelial cells (HUVECs) to cobalt chloride ($CoCl_2$). In addition, we show that silencing of YAP expression significantly prevented the fibrotic process in a laser-induced CNV mouse model.

MATERIALS AND METHODS

Ethical Approval Eight-week-old male C57BL/6J mice weighing 19-25 g were purchased from SLAC Laboratory Animal Co., Ltd. (Shanghai, China). The Animal Ethics Committee of Fudan University approved all experimental protocols involving animals. Animals were handled in accordance with The Association for Research in Vision and Ophthalmology statement "Use of Animals in Ophthalmology and Vision Research". Before performing experimental operations, all animals were acclimatized for at least 7d.

Chemicals and Reagents $CoCl_2$ was purchased from Sigma-Aldrich (St. Louis, MO, USA). Small molecule inhibitors YC-1 (Lificiguat, a specific inhibitor of HIF-1α), CA3 (CIL56, an inhibitor of YAP), and XMU-MP-1 (an inhibitor of Hippo kinase MST1/2, which activates YAP) were purchased from Selleck Chemicals (Houston, TX, USA). Antibodies for YAP1, HIF-1α, α-SMA, CD31, and Snail were obtained from Huaan Biotechnology Company (Hangzhou, China). Antibodies for phosphorylated YAP, vimentin, and zonula occludens 1 (ZO-1) were purchased from Cell Signaling Technology (Beverly, MA, USA), while the antibody for β-actin was from Beyotime Institute of Biotechnology (Shanghai, China). Complete endothelial cell medium (ECM) containing 5% fetal bovine serum (FBS) and endothelial cell growth supplement was purchased from ScienCell Research Laboratory (Carlsbad, CA, USA).

Cell Culture Primary HUVECs were obtained from ScienCell and cultured in ECM at 37℃ and 5% CO_2 in a humidified incubator. Cells were used in experiments between passages 3 and 7.

Chemical Anoxic Treatment HUVECs were plated in six-well plates and cultured in an incubator at 37℃ and 5% CO_2 with normal oxygen until they reached confluency 70%. Subsequently, the medium was exchanged for medium containing 2% FBS and varying concentrations (0-500 μmol/L) of $CoCl_2$. After 24h of culture, HUVECs were used for additional measurements.

Based on previous studies, the small molecule inhibitors CA3, YC-1, and XMU-MP-1 were prepared at a concentration of 1 mmol/L in dimethyl sulfoxide, and then adjusted to a final concentration of 1 μmol/L with ECM containing 2% FBS for treatment of cells[20-22].

Choroidal Neovascularization Model Induced by Laser Photocoagulation The CNV mouse model was induced by laser photocoagulation according to a previously published protocol[23-24]. Briefly, C57BL/6J mice were anesthetized with 2% sodium pentobarbital (50 mg/kg, Sigma-Aldrich), and the pupils of both eyes were dilated with 1% topiramate (Alcon Laboratories, Fort Worth, TX, USA). Laser photocoagulation was performed on the fundus of mice (532-nm wavelength, 100-mW power, 50-μm spot size, 100-ms duration). Four to six laser spots were made around the optic nerve to cause damage. Microscopy revealed the appearance of bubbles in all laser burns. Spots containing bleeding or an absence of bubbles at the laser site were excluded from subsequent experiments. According to established protocols, cholesterol-modified small interfering RNA (siRNA) targeting YAP or a scramble sequence (Ribobio, Guangzhou, China) were intravitreally injected at 0.1 nmol in one eye of adult mice on day 1 (d1) and d14 after photocoagulation[25-26]. Mice were sacrificed at d7.

Quantitative Real-time PCR Total RNA was extracted using Trizol reagent (Takara Bio, Shiga, Japan) and synthesized into cDNA using a reverse transcription kit. Amplification experiments were performed using a SYBR

green kit (Takara Bio) according to the manufacturer's instructions. Primer sequences were as follows: YAP1, 5'-GAACAATGACGACCAATAGCTC-3' (sense) and 5'-TAGTCCACTGTCTGTACTCTCA-3' (antisense); HIF-1α, 5'-AGTTCCGCAAGCCCTGAAAGC-3' (sense) and 5'-TCAGTGGTGGCAGTGGTAGTGG-3' (antisense); β-actin, 5'-ACCCACACTGTGCCCATCTA-3' (sense) and 5'-GCCACAGGATTCCATACCCA-3' (antisense). β-actin was used as an internal reference gene to calculate the relative expression of target genes using the $2^{-\Delta\Delta Ct}$ method for three independent experimental repeats.

Western Blotting Cell lysates were prepared using cell lysis buffer containing phosphatase inhibitors. The resulting protein concentrations were determined using a bicinchoninic acid protein assay. After completely separating 40 μg of total protein sample per lane, proteins were transferred to a polyvinylidene fluoride membrane and blocked with 10% skimmed milk for 1h. Next, membranes were incubated with one or more of the following primary antibodies overnight at 4℃: YAP1 (1:1000), phospho-YAP (1:1000), HIF-1α (1:500), α-SMA (1:1000), CD31 (1:500), vimentin (1:1000), ZO-1 (1:1000), Snail (1:1000), and β-actin (1:1000). Subsequently, membranes were reacted with appropriate secondary antibodies for 1h, then detected and observed using an enhanced chemiluminescence substrate kit. The gray value of each target band was analyzed by Image J software (https://imagej.nih.gov/ij/) using β-actin as an internal reference. This experiment was repeated three times independently.

Immunofluorescent Staining After aspirating the medium and washing three times with phosphate-buffered saline (PBS, 3min each wash), cells were fixed with 4% polyoxymethylene solution for 15min at room temperature and washed again. Next, cells were permeabilized with 0.5% Triton X-100 at room temperature for 30min and washed again three times (3min each) with PBS. Cells were blocked with 5% bovine serum albumin (BSA) for 30min and then immediately incubated with diluted primary antibody (YAP1, 1:50; CD31, 1:20; α-SMA, 1:50) overnight at 4℃. Subsequently, cells were incubated with a fluorescent secondary antibody for 1h, washed three times (3min each) with PBS, and incubated with 4′,6-diamidino-2-phenylindole (DAPI) for 15min in the dark. Images were acquired with an upright BX63 fluorescence microscope (Olympus, Tokyo, Japan). This experiment was repeated three times.

CCK8 Assay After exposing HUVECs in a 96-well plate to $CoCl_2$ for 24h, 100 μL of high-sensitivity CCK-8 reagent from a cell proliferation detection kit (Keygen Biotech, Jiangsu Province, China) was added to each well for incubation at 37℃ for 3h. Subsequently, the absorbance value of each well was measured at a 450-nm wavelength to assess cell viability. Three replicates were used for each of three independent experiments.

Scratch Wound-healing Assay After cells plated in six-well plates reached confluency, they were streaked with a sterile 200-μL pipette tip and washed three times with PBS. Next, serum-free medium (control) or serum-free medium containing $CoCl_2$ alone or in combination with inhibitors was added to the plate. Scratch widths were observed and photographed under an inverted BX63 microscope after 0, 24, 32, and 48h of culture. The distance between scratches was measured using Image-Pro Plus 6.0 software (Media Cybernetics, Rockville, MD, USA). This experiment was repeated three times.

Paraffin Section Immunofluorescence Slices were placed at room temperature for 10min and then immersed in xylene for 15min, which was repeated twice. After deparaffinizing paraffin sections in a gradient series of ethanol, slices were incubated with citric acid antigen retrieval solution in a microwave oven for 15min under low heat to retrieve antigens. After washing and cooling, sections were washed three times with PBS. To block nonspecific binding, 5% BSA solution was added dropwise to the tissue and incubated for 30min at room temperature. After shaking off the blocking solution, prepared primary antibody solutions were dropped onto the tissue section, which was put in a humid box and incubated overnight at 4℃. The next day, sections were immersed in PBS and washed three times. After drying, fluorescent secondary antibody was added dropwise and incubated for 1h at room temperature in the dark. After placing slices in PBS and washing three times (5min each), nuclear staining was performed by incubating slice with DAPI at room temperature for 15min. Sections were again placed in PBS and washed three times. Finally, an appropriate amount of anti-quenching agent was added and sections were observed and imaged by fluorescence microscopy.

Statistical Analysis Statistical analysis was performed using SigmaPlot 14.0 (Systat Software, San Jose, CA, USA). Significant statistical differences were determined by Student's *t*-test or one-way ANOVA followed by Holm-Sidak posthoc test. A P value <0.05 was considered significant difference.

RESULTS

EndMT of HUVECs Stimulated by Hypoxia Previous reports showed hypoxia that can induce EndMT of endothelial cells. Here, we stimulated HUVECs with $CoCl_2$ to establish a hypoxia model *in vitro*. To verify whether endothelial cells underwent changes characteristic of EndMT, we detected expression levels of HIF-1α, endothelial cell markers (CD31 and ZO-1), and mesenchymal cell markers (α-SMA, vimentin, and Snail) by Western blotting. Expression of HIF-1α and mesenchymal cell markers were upregulated by exposure to $CoCl_2$ in a dose-dependent manner (Figure 1). Conversely,

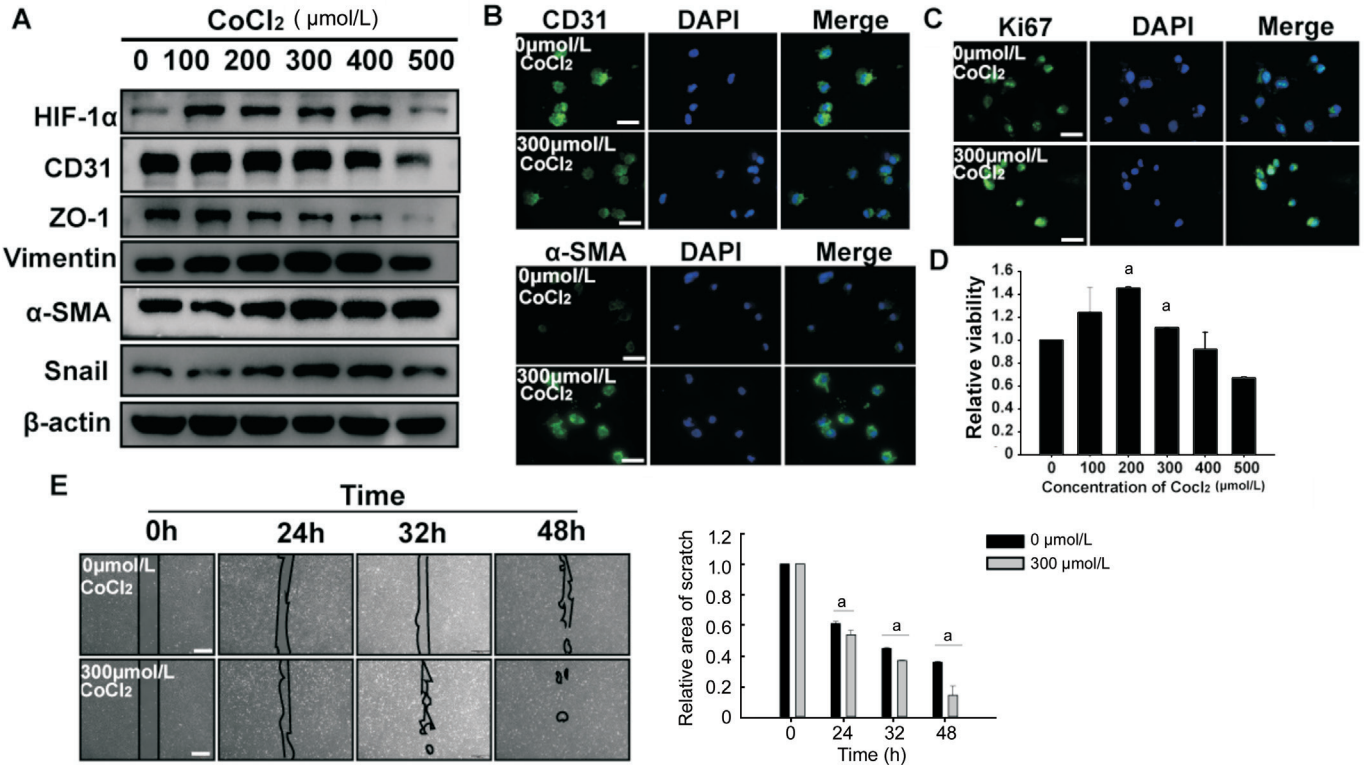

Figure 1 Hypoxia promoted EndMT of HUVECs A: HUVECs undertook a 24h culture with increasing doses of $CoCl_2$ (0-500 μmol/L). The levels of HIF-1α, Snail, endothelial cell markers and mesenchymal cell markers were measured by Western blotting. B, C: HUVECs were treated with 300 μmol/L $CoCl_2$ for 24h. CD31 (green), α-SMA (green) in HUVECs were observed by immunofluorescence staining, and Ki67 (green) immunostaining was used for analysis of proliferative capacity of hypoxic HUVECs. Scale bar represents 100 μm. D: The effect of different concentrations of $CoCl_2$ at 0-500 μmol/L on the proliferation of HUVECs was detected by CCK8 assay. E: Scratch healing experiments performed the migration ability of hypoxic HUEVCs. Scale bar represents 500 μm. All the results were expressed as mean±SD (n=3). $^aP<0.05$. EndMT: Endothelial-to-mesenchymal transition; HUVECs: Human umbilical vein endothelial cells; α-SMA: α smooth muscle actin.

endothelial cell markers were downregulated in HUVECs exposed to $CoCl_2$. Because these changes were most pronounced at a concentration of 300 μmol/L $CoCl_2$, we selected this concentration for subsequent experiments, as described in a previous study[27]. As shown in Figure 1, immunofluorescence microscopy results were consistent with trends observed by western blotting. Moreover, the proliferative ability and migration capacity of HUVECs exposed to $CoCl_2$ (300 μmol/L) was significantly increased compared with the control group, as indicated by Ki67 staining, CCK8 assay, and scratch wound-healing assay (Figure 1). In summary, we found that HUVECs undergo EndMT in response to $CoCl_2$-induced hypoxia.

Increased Total Expression and Transcriptional Activity of YAP in HUVECs by Hypoxia To evaluate YAP expression in HUVECs under hypoxia, we analyzed transcript and protein levels of YAP in HUVECs exposed to different concentrations of $CoCl_2$. Western blot and qPCR analysis showed that $CoCl_2$ elicited a significant increase of YAP expression, consistent with changes in HIF-1α (Figure 2). To further quantify the transcriptional activity of YAP under hypoxia, we examined levels of YAP phosphorylation and expression of connective tissue growth factor (CTGF), a target of YAP, by Western blotting. When HUVECs were exposed to 0-500 μmol/L of $CoCl_2$, the phosphorylation level of YAP-Ser127 decreased in a concentration-dependent manner. Moreover, CTGF expression was upregulated by $CoCl_2$ exposure, consistent with changes in HIF-1α. Immunofluorescence staining also showed that $CoCl_2$ promoted YAP expression and nuclear translocation in HUVECs (Figure 2). Therefore, both total YAP expression and its transcriptional activity may be of great importance in hypoxia-induced EndMT of HUVECs.

YAP, a Positive Regulator of Hypoxia-Induced EndMT in HUVECs To further clarify whether YAP influenced EndMT, HUVECs were exposed to $CoCl_2$ alone or in combination with CA3, a small molecule inhibitor of YAP. CA3 has a potent inhibitory effect on YAP transcriptional activity[21]. Western blotting and qPCR results showed that CA3 pretreatment could reverse $CoCl_2$-induced upregulated expression of YAP, CTGF, α-SMA, vimentin, and Snail, as well as downregulated expression of CD31 and ZO-1. Immunofluorescence staining revealed the same trend for YAP expression. Ki67 staining and scratch wound-healing assay results showed that the proliferative and migratory abilities of HUVECs exposed to $CoCl_2$ combined with CA3 was lower than cells exposed to $CoCl_2$ alone (Figure 3).

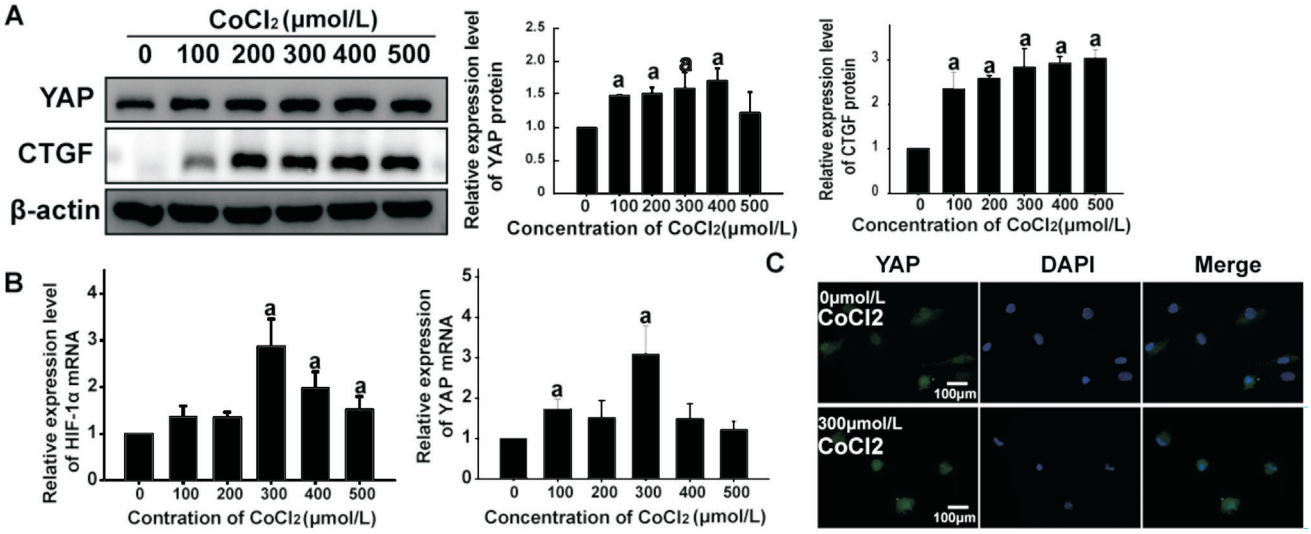

Figure 2 Hypoxia increased the expression of total YAP and its transcriptional activity in HUVECs A: Expression level of YAP, phosphorylated YAP and its target molecular CTGF in HUVECs treated with $CoCl_2$ at concentrations of 0-500 μmol/L for 24h was analyzed by Western blotting. Quantitative analysis showed that the levels of YAP and CTGF protein were significantly higher in $CoCl_2$ treated group than that in control group, and phosphorylation of YAP was decreased, $^aP<0.05$. B: qPCR analysis showed that HIF-1α was significantly increased by $CoCl_2$, as well as YAP mRNA. C: HUEVCs were treated with 300 μmol/L $CoCl_2$ for 24h, and YAP was immunolabeled (green). Scale bar represents 100 μm. The fluorescence intensity of the experimental group was more than that of the control group. All the results were expressed as mean±SD (n=3). $^aP<0.05$. YAP: Yes-associated protein; CTGF: Connective tissue growth factor; HUVECs: Human umbilical vein endothelial cells; HIF-1α: Hypoxia-inducible factor-1α.

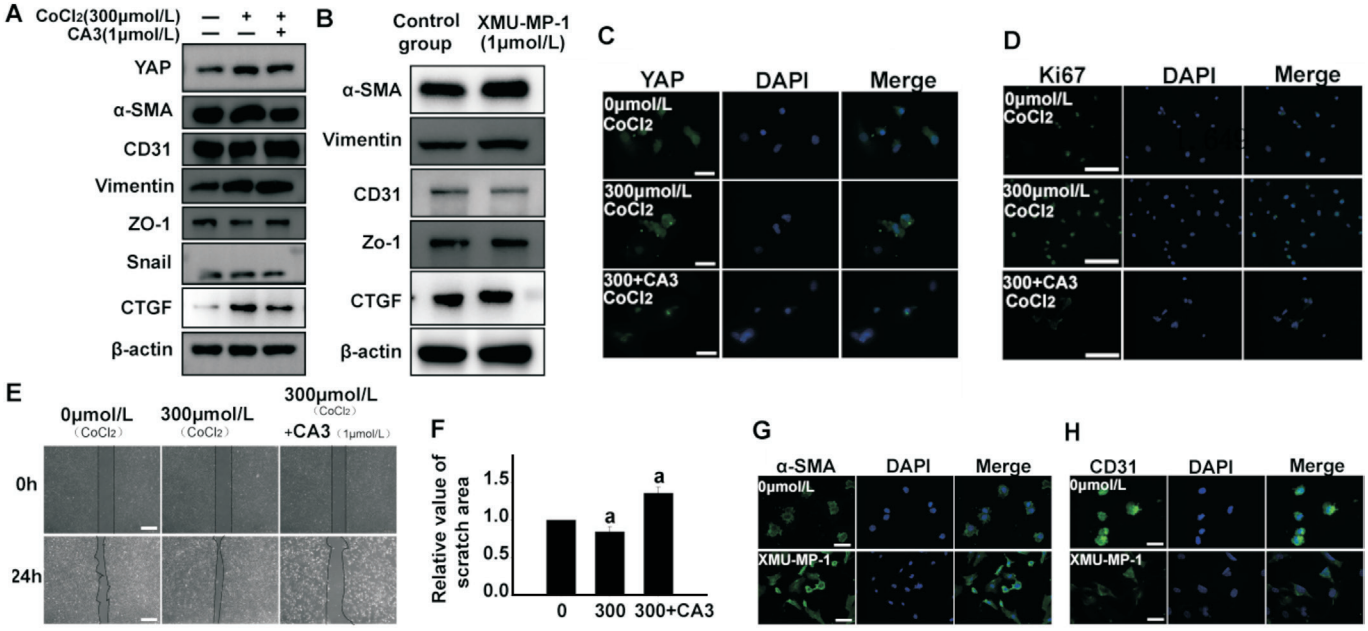

Figure 3 Inhibition of total YAP attenuated the hypoxia-induced EndMT in HUVECs and inhibiting phosphorylation of YAP induced the hypoxia-induced EndMT in HUVECs A: HUVECs treated with 300 μmol/L $CoCl_2$ and YAP small molecule inhibitor CA3 (1 μmol/L) for 24h. Proteins of EndMT were detected by Western blotting. B: HUVECs were treated with XMU-MP-1 inhibitor alone for 24h, and the expression levels of α-SMA, vimentin, CD31 and ZO-1 were analyzed by Western blotting. C: HUVECs treated with 300 μmol/L $CoCl_2$ and YAP small molecule inhibitor CA3 (1 μmol/L) for 24h. YAP was observed by immunostaining. Scale bar represents 100 μm. D: Analysis of proliferative capacity of hypoxic HUVECs using Ki67 (green) and DAPI (blue) immunostaining. Scale bar represents 200 μm. E-F: Scratch healing experiments were performed to examine the effect of CA3 on the migration ability. Scale bar represents 500 μm. G, H: α-SMA and CD31 (green) were observed by immunofluorescence staining. Inhibition of YAP phosphorylation by XMU-MP-1 increased the expression level of α-SMA and inhibited the expression of CD31 compared to the control group. The results showed inhibition of YAP resulted in a significant increase in the scratch area at 24h compared to the $CoCl_2$ treated group. Scale bar represents 100 μm. All the results were expressed as mean±SD (n=3). $^aP<0.05$. YAP: Yes-associated protein; EndMT: Endothelial-to-mesenchymal transition; HUVECs: Human umbilical vein endothelial cells; α-SMA: α smooth muscle actin.

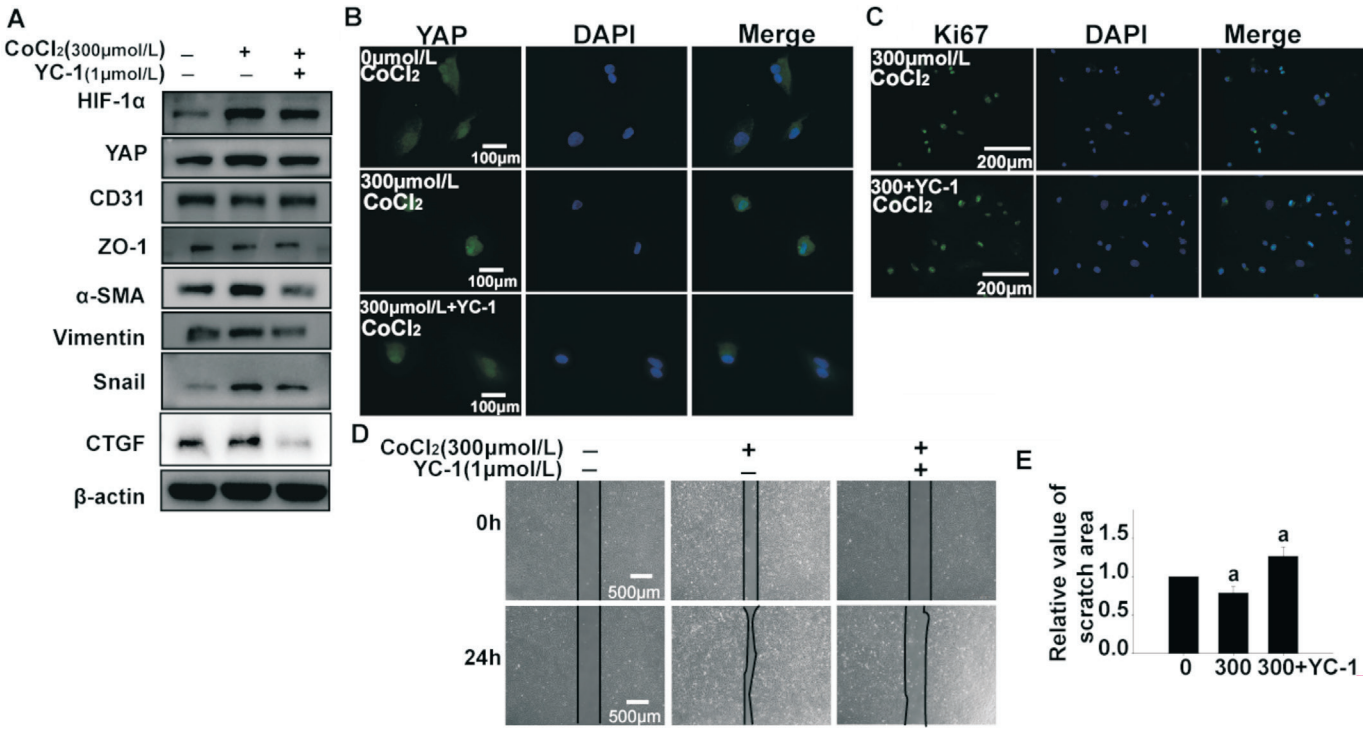

Figure 4 Inhibition of HIF-1α decreased the expression and transcriptional activity of YAP as well as EndMT in HUVECs, but inhibiting phosphorylation of YAP promoted the activity of YAP A: HUVECs were treated with 300 μmol/L $CoCl_2$ and YC-1 (1 μmol/L) for 24h. HIF-1α, YAP, CTGF and proteins of EndMT were detected by Western blotting. B: YAP was observed by immunostaining and scale bar represents 100 μm. C: Ki67 (green) and DAPI (blue) immunostaining was used to analyze proliferative capacity of hypoxic HUVECs. Scale bar represents 200 μm. D, E: Scratch healing experiments were performed to examine the effect of YC-1 on the migration ability of 300 μmol/L $CoCl_2$-induced hypoxic HUVECs. Scale bar represents 500 μm. All the results were expressed as mean±SD (n=3). $^aP<0.05$. HIF-1α: Hypoxia-inducible factor-1α; YAP: Yes-associated protein; EndMT: Endothelial-to-mesenchymal transition; HUVECs: Human umbilical vein endothelial cells; CTGF: Connective tissue growth factor.

Phosphorylation of YAP-Ser127 creates a binding consensus for 14-3-3 proteins that contributes to YAP entrapment and maintenance of YAP in an inactive state[28-29]. To clarify whether phosphorylation of YAP is involved in EndMT, HUVECs were treated with the MST1/2 inhibitor XMU-MP-1 for 24h under normoxia and analyzed for changes of endothelial and mesenchymal markers using Western blotting. We found that inhibiting YAP phosphorylation in endothelial cells increased expression levels of the mesenchymal markers α-SMA and vimentin, while inhibiting endothelial markers CD31 and ZO-1. The results of immunofluorescence staining were consistent with those of Western blotting (Figure 3). Collectively, these results suggest that YAP plays a significant role in hypoxia-induced EndMT of HUVECs.

Decreased YAP Expression and Transcriptional Activity as Well as EndMT in HUVECs by Inhibiting HIF-1α HIF-1α is proven to be essential for expression and nuclear translocation of YAP[30]. Therefore, we exposed HUVECs to $CoCl_2$ and YC-1, a small molecule inhibitor of HIF-1α. As shown in Figure 4, $CoCl_2$-induced HIF-1α expression was reversed by YC-1. As predicted, expression of mesenchymal markers α-SMA, vimentin, and Snail were significantly decreased, while expression of endothelial markers CD31 and ZO-1 showed an upward trend. Moreover, expression of YAP and its target molecule CTGF was simultaneously decreased. Immunofluorescence staining of YAP showed a consistent trend. Furthermore, both the proliferative and migratory abilities of HUVECs were decreased by YC-1 (Figure 4). These results indicate that HIF-1α is a key mediator of YAP expression and transcriptional activity, as well as hypoxia-induced EndMT of HUVECs.

Attenuating Subretinal Fibrosis in a Laser-induced CNV Mouse Model by YAP Silence To clarify the role of YAP on EndMT and subsequent fibrosis in CNV, we constructed a mouse CNV model using laser-induced injury. On the 35th day after laser injury, expression levels of YAP and mesenchymal cell markers α-SMA and vimentin were detected in the mouse pigment epithelium-choroid complex. Western blot analysis revealed that expression of YAP, α-SMA, and vimentin were all upregulated in the CNV group. Co-staining of COL1A1 and CD31 reflected the occurrence of EndMT in subretinal fibrosis of the CNV model (Figure 5). Therefore, we speculate that YAP promotes the subretinal fibrosis that occurs subsequent to CNV.

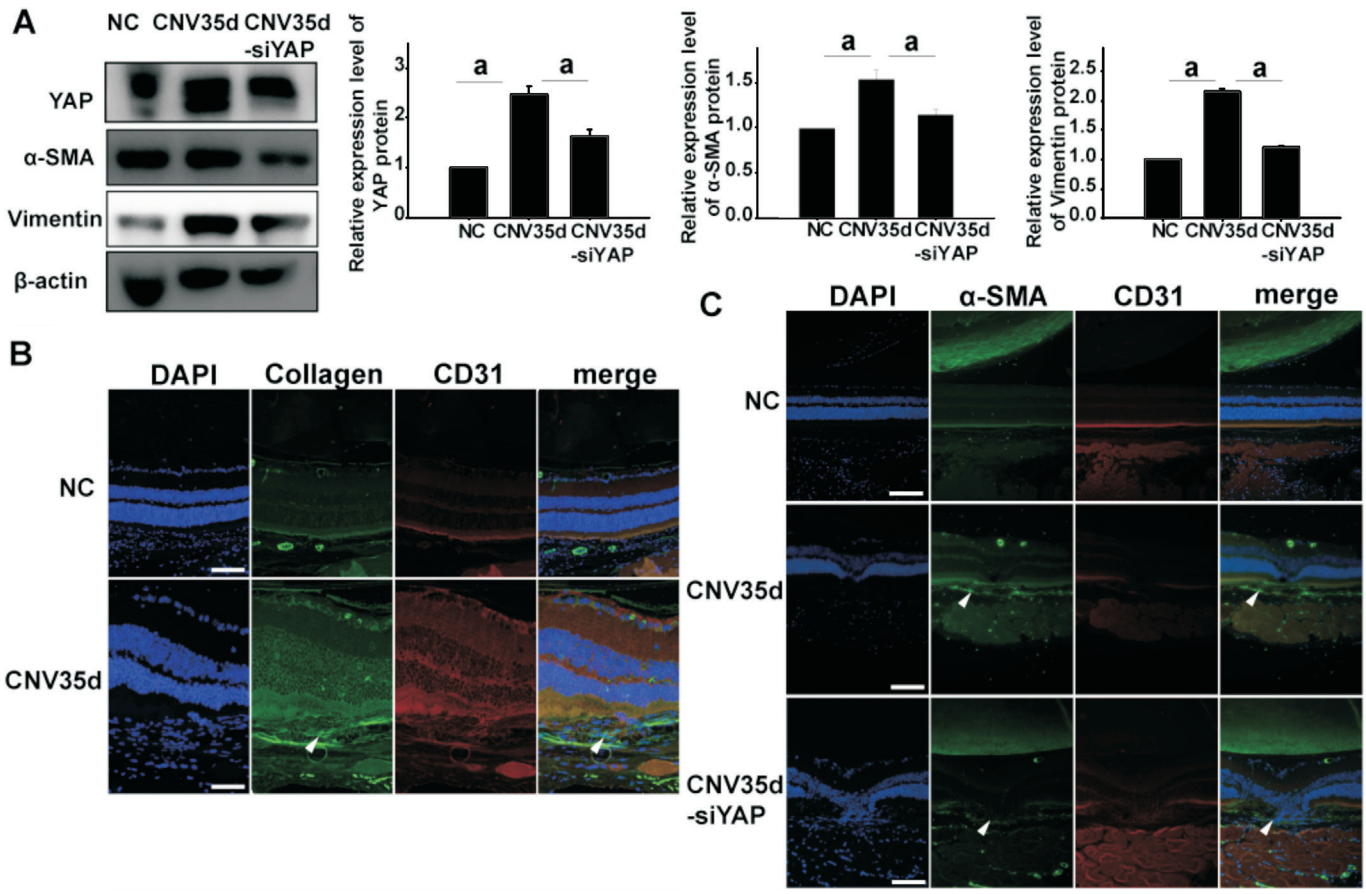

Figure 5 Increased expression of YAP and mesenchymal cell markers α-SMA, vimentin and collagen in CNV tissues A: Immunoblotting for YAP and α-SMA, vimentin protein in the retina and the retinal pigment epithelium-choroid complex in CNV model at 35th day, CNV model mice treated by vitreous injection of siRNA YAP and control group; B: Immunofluorescence staining of paraffin sections show that expression of collagen increased in CNV model at 35th day. Scale bar represents 100 μm; C: Immunofluorescence staining of paraffin sections show that expression of α-SMA increased in CNV model at 35th day and CD31 expression was decreased. After vitreous injection of siRNA YAP treatment, these changes were reversed. Scale bar represents 100 μm. YAP: Yes-associated protein; α-SMA: α smooth muscle actin; CNV: Choroidal neovascularization.

To further verify our hypothesis, mice were intravitreally injected with siRNA YAP on the second day after injury, and the injection was repeated at 2wk after laser photocoagulation. On day 35 after CNV model establishment, we extracted the retina and choroid tissue complex, and performed paraffin sectioning of the eyeball. Western blot results showed that intravitreal injection of siRNA YAP could reverse $CoCl_2$-induced upregulation of YAP and mesenchymal cell markers α-SMA and vimentin. Immunofluorescence staining results were consistent with previous studies (Figure 5). Taken together, these findings indicate that silencing of YAP inhibits EndMT in subretinal fibrosis of a laser-induced CNV mouse model.

DISCUSSION

As the main cause of visual impairment in elderly individuals, wet AMD has attracted widespread attention. CNV is a feature of neovascular AMD, also known as wet AMD[1]. Immature blood vessels in CNV cannot supply oxygen or nutrients at the level of normal blood vessels, causing further tissue hypoxia. Moreover, repeated leakage and bleeding from immature blood vessels can damage the retina by causing subretinal fibrosis. Therefore, CNV can complicate AMD, leading to severe vision loss and blindness[31]. Inhibiting the occurrence of fibrosis in patients with wet AMD is vital to maintain their visual function. Therefore, further research on mechanisms that promote the occurrence of fibrosis is necessary. In this study, we clarified the importance of YAP activity in hypoxia-induced EndMT and subretinal fibrosis of a laser-induced CNV model. Using *in vitro* experiments, we verified that YAP expression and activity was increased in HUVECs under hypoxic stimulation. Our work further revealed that YAP is necessary for hypoxia-induced EndMT of HUVECs. Finally, silencing of YAP inhibited EndMT associated with subretinal fibrosis in the laser-induced CNV model, indicating YAP might be a new and effective therapeutic target for CNV therapy.

As the main effector of cells under hypoxic conditions, HIF-1α is responsible for regulating various cellular responses[32]. Because of its role in stabilizing HIF-1α, $CoCl_2$ has become

one of the most commonly used hypoxia mimics[33]. Studies have reported that hypoxia can increase expression of HIF-1α and YAP in tumor cells[34], and promotes nuclear localization of YAP with reduced phosphorylation levels by inhibiting Hippo signaling[35]. However, reports describing the relationship between HIF-1α and YAP are inconsistent. For example, Zhang *et al*[35] found that YAP binds to HIF-1α and maintains its protein stability; in contrast, Dai *et al*[36] revealed that hypoxia induced nuclear translocation and accumulation of YAP independent of HIF-1α, as indicated by manipulations of HIF-1α abundance with $CoCl_2$ having no effect on total or phosphorylated levels of YAP. This discrepancy suggests potential bidirectional regulation between HIF-1α and YAP. In this study, the HIF-1α inhibitor YC-1 was used to clarify the regulatory effect of HIF-1α on YAP.

EndMT of both choroidal and retinal endothelial cells has been studied in numerous ocular angiogenic diseases, including AMD, proliferative diabetic retinopathy, and retinopathy of prematurity[3,37]. In the present study, expression of endothelial markers CD31 and ZO-1 was decreased, while that of mesenchymal markers α-SMA, vimentin, and Snail was increased in HUVECs after hypoxia, consistent with results observed for cells exposed to 1% O_2[38]. More importantly, we also investigated the impact of YAP on HIF-1α-meditated EndMT. Our results reveal that pharmacological inhibition or genetic depletion of YAP could attenuate EndMT of HUVECs *in vitro*, as well as fibrosis of a laser-induced CNV mouse model *in vivo*. Savorani *et al*[16] recently provided novel evidence that YAP acts as SMAD3 transcriptional co-factor by preventing its phosphorylation, thus protecting against TGFβ-induced EndMT. Given that Snail is an important regulator of hypoxia-induced EndMT[39-40], whether YAP influences expression or nuclear transcription of Snail needs further elucidation.

With regard to biological function, we observed that upregulation of YAP was accompanied by increases in the proliferative capacity and migratory ability of HUVECs. Endothelial cells undergoing EndMT exhibited higher proliferation and migration abilities, both directly through transformation into smooth muscle-like cells and indirectly through paracrine secretion[41]. In addition, the mesenchymal transition regulator Snail functions to promote cell proliferation and migration[42]. Thus, we speculate that promotion of endothelial cell proliferation and migration induced by YAP may be attributed to EndMT regulation.

In conclusion, the present study identified a critical role of the HIF-1α/YAP signaling axis in EndMT, which suggests that YAP may be an attractive target for treatment of AMD with the advantage of controlling both CNV and subretinal fibrosis.

ACKNOWLEDGEMENTS

We thank Liwen Bianji (Edanz) (www.liwenbianji.cn/) for editing the English text of a draft of this manuscript.

Authors' contributions: Zou R, Feng YF, Xu YH, Shen MQ and Zhang X performed the research; Yuan YZ designed the research study; and Zou R and Feng YF analyzed the data and prepared the manuscript.

Foundations: Supported by the National Natural Science Foundation of China (No.81970817; No.81873680).

Conflicts of Interest: Zou R, None; **Feng YF,** None; **Xu YH,** None; **Shen MQ,** None; **Zhang X,** None; **Yuan YZ,** None.

REFERENCES

1 Yeo NJY, Chan EJJ, Cheung C. Choroidal neovascularization: mechanisms of endothelial dysfunction. *Front Pharmacol* 2019;10:1363.

2 Wu D, Kanda A, Liu Y, Kase S, Noda K, Ishida S. Galectin-1 promotes choroidal neovascularization and subretinal fibrosis mediated via epithelial-mesenchymal transition. *FASEB J* 2019;33(2): 2498-2513.

3 Sun JX, Chang TF, Li MH, Sun LJ, Yan XC, Yang ZY, Liu Y, Xu WQ, Lv Y, Su JB, Liang L, Han H, Dou GR, Wang YS. SNAI1, an endothelial-mesenchymal transition transcription factor, promotes the early phase of ocular neovascularization. *Angiogenesis* 2018;21(3):635-652.

4 Sniegon I, Prieß M, Heger J, Schulz R, Euler G. Endothelial mesenchymal transition in hypoxic microvascular endothelial cells and paracrine induction of cardiomyocyte apoptosis are mediated via $TGF\beta_1$/SMAD signaling. *Int J Mol Sci* 2017;18(11):E2290.

5 Jiang R, Liao Y, Yang FH, Cheng YS, Dai XN, Chao J. SPIO nanoparticle-labeled bone marrow mesenchymal stem cells inhibit pulmonary EndoMT induced by SiO_2. *Exp Cell Res* 2019;383(1): 111492.

6 Piera-Velazquez S, Mendoza FA, Jimenez SA. Endothelial to mesenchymal transition (EndoMT) in the pathogenesis of human fibrotic diseases. *J Clin Med* 2016;5(4):E45.

7 Chen CL, Chou KJ, Fang HC, Hsu CY, Huang WC, Huang CW, Huang CK, Chen HY, Lee PT. Progenitor-like cells derived from mouse kidney protect against renal fibrosis in a remnant kidney model *via* decreased endothelial mesenchymal transition. *Stem Cell Res Ther* 2015;6:239.

8 Zhang B, Niu W, HY, Liu ML, Luo Y, Li ZC. Hypoxia induces endothelial-mesenchymal transition in pulmonary vascular remodeling. *Int J Mol Med* 2018:42(1):270-278.

9 Huang MG, Liu TR, Ma PH, Mitteer RA Jr, Zhang ZT, Kim HJ, Yeo E, Zhang D, Cai PQ, Li CS, Zhang L, Zhao BT, Roccograndi L, O'Rourke DM, Dahmane N, Gong YQ, Koumenis C, Fan Y. C-met-mediated endothelial plasticity drives aberrant vascularization and chemoresistance in glioblastoma. *J Clin Invest* 2016;126(5): 1801-1814.

10 Li ZY, Li XL, Zhu YQ, Chen QS, Li BG, Zhang FX. Protective effects of acetylcholine on hypoxia-induced endothelial-to-mesenchymal transition in human cardiac microvascular endothelial cells. *Mol Cell Biochem* 2020;473(1-2):101-110.

11 Hong WJ, Guan KL. The YAP and TAZ transcription co-activators: key downstream effectors of the mammalian Hippo pathway. *Semin Cell Dev Biol* 2012;23(7):785-793.

12 Totaro A, Panciera T, Piccolo S. YAP/TAZ upstream signals and downstream responses. *Nat Cell Biol* 2018;20(8):888-899.

13 Ling HH, Kuo CC, Lin BX, Huang YH, Lin CW. Elevation of YAP promotes the epithelial-mesenchymal transition and tumor aggressiveness in colorectal cancer. *Exp Cell Res* 2017;350(1): 218-225.

14 Han Q, Kremerskothen J, Lin XY, Zhang XP, Rong XZ, Zhang D, Wang EH. WWC_3 inhibits epithelial-mesenchymal transition of lung cancer by activating Hippo-YAP signaling. *Onco Targets Ther* 2018;11:2581-2591.

15 Park J, Kim DH, Shah SR, Kim HN, Kshitiz, Kim P, Quiñones-Hinojosa A, Levchenko A. Switch-like enhancement of epithelial-mesenchymal transition by YAP through feedback regulation of WT1 and Rho-family GTPases. *Nat Commun* 2019;10(1):2797.

16 Savorani C, Malinverno M, Seccia R, Maderna C, Giannotta M, Terreran L, Mastrapasqua E, Campaner S, Dejana E, Giampietro C. A dual role of YAP in driving TGFβ-mediated endothelial-to-mesenchymal transition. *J Cell Sci* 2021;134(15):jcs251371.

17 Ren YF, Zhang YW, Wang L, He FQ, Yan ML, Liu XH, Ou YY, Wu QK, Bi T, Wang SY, Liu J, Ding BS, Wang L, Qing J. Selective targeting of vascular endothelial YAP activity blocks EndMT and ameliorates unilateral ureteral obstruction-induced kidney fibrosis. *ACS Pharmacol Transl Sci* 2021;4(3):1066-1074.

18 Li J, Yao M, Zhu X, Li Q, He J, Chen L, Wang W, Zhu C, Shen T, Cao R, Fang C. YAP-induced endothelial-mesenchymal transition in oral submucous fibrosis. *J Dent Res* 2019;98(8):920-929.

19 Zhang HY, Liu Y, Yan LX, Du W, Zhang XD, Zhang M, Chen H, Zhang YF, Zhou JQ, Sun HL, Zhu DL. Bone morphogenetic protein-7 inhibits endothelial-mesenchymal transition in pulmonary artery endothelial cell under hypoxia. *J Cell Physiol* 2018;233(5):4077-4090.

20 Yeo EJ, Chun YS, Cho YS, Kim J, Lee JC, Kim MS, Park JW. YC-1:a potential anticancer drug targeting hypoxia-inducible factor 1. *J Natl Cancer Inst* 2003;95(7):516-525.

21 Song SM, Xie M, Scott AW, Jin JK, Ma L, Dong XC, Skinner HD, Johnson RL, Ding S, Ajani JA. A novel YAP1 inhibitor targets CSC-enriched radiation-resistant cells and exerts strong antitumor activity in esophageal adenocarcinoma. *Mol Cancer Ther* 2018;17(2):443-454.

22 Fan FQ, He ZX, Kong LL, Chen QH, Yuan Q, Zhang SH, Ye JJ, Liu H, Sun XF, Geng J, Yuan LZ, Hong LX, Xiao C, Zhang WJ, Sun XH, Li YZ, Wang P, Huang LH, Wu XR, Ji ZL, Wu Q, Xia NS, Gray NS, Chen LF, Yun CH, Deng XM, Zhou DW. Pharmacological targeting of kinases MST1 and MST2 augments tissue repair and regeneration. *Sci Transl Med* 2016;8(352):352ra108.

23 Yan ZZ, Shi HH, Zhu RR, Li LL, Qin B, Kang LH, Chen H, Guan HJ. Inhibition of YAP ameliorates choroidal neovascularization via inhibiting endothelial cell proliferation. *Mol Vis* 2018;24:83-93.

24 Wong CG, Taban M, Osann K, Ross-Cisneros FN, Bruice TC, Zahn G, You T. Subchoroidal release of VEGF and bFGF produces choroidal neovascularization in rabbit. *Curr Eye Res* 2017;42(2):237-243.

25 Feng YF, Wang J, Yuan YZ, Zhang X, Shen MQ, Yuan F. miR-539-5p inhibits experimental choroidal neovascularization by targeting CXCR7. *FASEB J* 2018;32(3):1626-1639.

26 Feng YF, Zou R, Zhang X, Shen MQ, Chen XP, Wang J, Niu WR, Yuan YZ, Yuan F. YAP promotes ocular neovascularization by modifying $PFKFB_3$-driven endothelial glycolysis. *Angiogenesis* 2021;24(3):489-504.

27 Liu XJ, Zhu MH, Yang XW, Wang Y, Qin B, Cui C, Chen H, Sang AM. Inhibition of RACK1 ameliorates choroidal neovascularization formation *in vitro* and *in vivo*. *Exp Mol Pathol* 2016;100(3):451-459.

28 Basu S, Totty NF, Irwin MS, Sudol M, Downward J. Akt phosphorylates the Yes-associated protein, YAP, to induce interaction with 14-3-3 and attenuation of p73-mediated apoptosis. *Mol Cell* 2003;11(1):11-23.

29 Moon S, Kim W, Kim S, Kim Y, Song Y, Bilousov O, Kim J, Lee T, Cha B, Kim M, Kim H, Katanaev VL, Jho EH. Phosphorylation by NLK inhibits YAP-14-3-3-interactions and induces its nuclear localization. *EMBO Rep* 2017;18(1):61-71.

30 Li H, Li XJ, Jing XZ, Li M, Ren Y, Chen JY, Yang CH, Wu H, Guo FJ. Hypoxia promotes maintenance of the chondrogenic phenotype in rat growth plate chondrocytes through the HIF-1α/YAP signaling pathway. *Int J Mol Med* 2018;42(6):3181-3192.

31 Nagai N, Oike Y, Izumi-Nagai K, Urano T, Kubota Y, Noda K, Ozawa Y, Inoue M, Tsubota K, Suda T, Ishida S. Angiotensin II type 1 receptor-mediated inflammation is required for choroidal neovascularization. *Arterioscler Thromb Vasc Biol* 2006;26(10):2252-2259.

32 Semenza GL. HIF-1 and mechanisms of hypoxia sensing. *Curr Opin Cell Biol* 2001;13(2):167-171.

33 Muñoz-Sánchez J, Chánez-Cárdenas ME. The use of cobalt chloride as a chemical hypoxia model. *J Appl Toxicol* 2019;39(4):556-570.

34 Greenhough A, Bagley C, Heesom KJ, Gurevich DB, Gay D, Bond M, Collard TJ, Paraskeva C, Martin P, Sansom OJ, Malik K, Williams AC. Cancer cell adaptation to hypoxia involves a HIF-GPRC5A-YAP axis. *EMBO Mol Med* 2018;10(11):e8699.

35 Zhang XD, Li Y, Ma YB, Yang L, Wang T, Meng X, Zong ZH, Sun X, Hua XD, Li HY. Yes-associated protein (YAP) binds to HIF-1α and sustains HIF-1α protein stability to promote hepatocellular carcinoma cell glycolysis under hypoxic stress. *J Exp Clin Cancer Res* 2018;37(1):216.

36 Dai XY, Zhuang LH, Wang DD, Zhou TY, Chang LL, Gai RH, Zhu DF, Yang B, Zhu H, He QJ. Nuclear translocation and activation of YAP by hypoxia contributes to the chemoresistance of SN38 in hepatocellular carcinoma cells. *Oncotarget* 2016;7(6):6933-6947.

37 Abu El-Asrar AM, de Hertogh G, van den Eynde K, Alam K, van Raemdonck K, Opdenakker G, van Damme J, Geboes K, Struyf S. Myofibroblasts in proliferative diabetic retinopathy can originate from infiltrating fibrocytes and through endothelial-to-mesenchymal transition (EndoMT). *Exp Eye Res* 2015;132:179-189.

38 Liu YH, Zou J, Li BG, Wang YQ, Wang DL, Hao YQ, Ke X, Li XX. RUNX3 modulates hypoxia-induced endothelial-to-mesenchymal transition of human cardiac microvascular endothelial cells. *Int J Mol Med* 2017;40(1):65-74.

39 Xu XB, Tan XY, Tampe B, Sanchez E, Zeisberg M, Zeisberg EM. Snail is a direct target of hypoxia-inducible factor 1α (HIF1α) in hypoxia-induced endothelial to mesenchymal transition of human coronary endothelial cells. *J Biol Chem* 2015;290(27): 16653-16664.

40 Tang H, Babicheva A, McDermott KM, *et al*. Endothelial HIF-2α contributes to severe pulmonary hypertension due to endothelial-to-mesenchymal transition. *Am J Physiol Lung Cell Mol Physiol* 2018;314(2):L256-L275.

41 Suzuki T, Carrier EJ, Talati MH, Rathinasabapathy A, Chen XP, Nishimura R, Tada YJ, Tatsumi K, West J. Isolation and characterization of endothelial-to-mesenchymal transition cells in pulmonary arterial hypertension. *Am J Physiol Lung Cell Mol Physiol* 2018;314(1):L118-L126.

42 Yang XY, Han MM, Han HB, Wang BJ, Li S, Zhang ZQ, Zhao W. Silencing Snail suppresses tumor cell proliferation and invasion by reversing epithelial-to-mesenchymal transition and arresting G2/M phase in non-small cell lung cancer. *Int J Oncol* 2017;50(4):1251-1260.